INTERNATIONAL JOURNAL OF HYDROGEN ENERGY 40 (2015) 5707–5714

Available online at www.sciencedirect.com

ScienceDirect

journal homepage: www.elsevier.com/locate/he

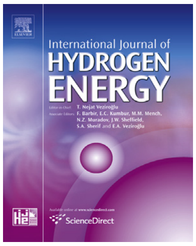

Spark-plasma-sintered barium zirconate based proton conductors for solid oxide fuel cell and hydrogen separation applications

Siwei Wang [a], Yufei Liu [b], Jian He [b], Fanglin Chen [c], Kyle S. Brinkman [a,*]

[a] Department of Materials Science and Engineering, Clemson University, Clemson, SC 29634, USA
[b] Department of Physics and Astronomy, Clemson University, Clemson, SC 29634, USA
[c] Department of Mechanical Engineering, University of South Carolina, Columbia, SC 29208, USA

ARTICLE INFO

Article history:
Received 15 January 2015
Received in revised form
24 February 2015
Accepted 25 February 2015
Available online 20 March 2015

Keywords:
Proton conductor
Solid oxide fuel cells
Hydrogen separation
Spark plasma sintering

ABSTRACT

Proton conducting ceramics exhibit high levels of bulk proton conductivity at intermediate temperatures (500–700 °C). However, this material class has not been widely utilized in energy conversion and storage applications due to the blocking behavior of the grain boundary proton conduction. A better understanding of proton conduction in these materials requires a systematic study of the sintering conditions that determine microstructure and ultimately the electrical properties. In this work, spark plasma sintering with high heating rates was employed to prepare a state-of-the-art $BaZr_{0.9}Y_{0.1}O_{3-\delta}$ (BZY) proton conductor for studies focused on the behavior of proton conduction at the grain boundary interfaces. The ceramics prepared by the SPS method resulted in an ultra-fine grain size of approximately 200 nm. The large grain boundary interfacial area was used as a “tool” to investigate the interfacial conduction in these materials systems. Samples displayed a lowered grain boundary conductivity and a higher activation energy compared with the literature results on conventionally prepared materials. The lower bulk conductivity is interpreted with reference to polymorphs of BZY sintered at different temperatures. The combined effect led to a lower total conductivity of the SPS densified BZY ceramics.

Copyright © 2015, Hydrogen Energy Publications, LLC. Published by Elsevier Ltd. All rights reserved.

Introduction

Proton conducting oxide materials have been extensively studied due to their unique proton conduction at intermediate temperatures (500–700 °C) [7,10,11,25,29,32]. This materials class has demonstrated potential for use as high temperature H_2 separation membranes to produce purified H_2, as well as for electrolytes in next generation proton conducting solid oxide fuel cells that operate at lower temperatures than the state-of-the-art oxygen ion conducting SOFCs [4,5,26,28,30,32–34]. Among the various compositions of proton conductors, the $BaZrO_3$ based compounds with different dopants and co-dopants have been widely investigated due to their high bulk proton conductivity and high chemical stability [14,20]. Although these proton conducting oxides possess high levels of bulk conductivity, in practice, the total conductivity of such

---

* *Corresponding author.*
E-mail address: ksbrink@clemson.edu (K.S. Brinkman).

http://dx.doi.org/10.1016/j.ijhydene.2015.02.116

0360-3199/Copyright © 2015, Hydrogen Energy Publications, LLC. Published by Elsevier Ltd. All rights reserved.

materials varies greatly depending on the synthesis methods employed. This implies that the microstructures, especially interfacial microstructures, play a key role in determining the overall performance [27]. Typically, large grained materials show a lower grain boundary resistance and a higher total conductivity. Highly resistive grain boundaries and potential space-charge induced segregations of acceptor dopants at the grain boundaries may play an important role [9]. The work outlined in this manuscript focused on the preparation methods that determine the microstructure of the materials, as well as the impact of the microstructure on the electrical properties.

Spark plasma sintering (SPS) provides a unique way of densifying materials at very low temperatures (at temperatures far below the melting point) via fast heating rates, which suppresses the grain growth during sintering, resulting in a refined microstructure. The lowered sintering temperature also avoids the evaporation of some volatile components during sintering. Different from conventional furnace sintering, SPS heats the materials by applying pressure and electric current directly to the sample simultaneously, so that dense ceramics can be obtained under uniform heating at relatively low sintering temperatures and in short processing times. The SPS method has been widely applied to various SOFC solid electrolytes to obtain dense sintered specimens, such as yttrium doped zirconia, $La_{0.9}Sr_{0.1}Ga_{0.8}Mg_{0.2}O_{3-\delta}$, samarium doped ceria, as well as barium zirconate [8,9,12,15,17]. The SPS process was observed to enhance the conductivity of electrolytes in some studies [8,15], while other investigations did not show any improvement in the conductivity [9,13]. Those studies observing an enhanced conductivity reported that ultrafine grain sizes resulted in a modification in the grain boundary characteristics. A change in the grain boundary behavior from a barrier, to a promoter of proton transport was hypothesized [15]. In addition, less impurities in the ceramic phase [12], or improved densification of the materials were offered as additional explanations for the observed results [8]. With regards to the grain boundary conductivity in particular, recent results have indicated that samples sintered at lower temperature possess smaller grain size and higher grain boundary resistivity [13]. Consequently, the sintering conditions of SPS impacts the microstructure and the conductivity of the resulting samples. In this work, the small grain size induced by SPS processing resulted in a large grain boundary area that was used as a "tool" to investigate the interfacial conduction in these materials systems.

In this paper, we investigated the state-of-the-art yttrium doped barium zirconate $BaZr_{0.9}Y_{0.1}O_{3-\delta}$ (BZY) proton conductor sintered by the SPS method. BZY powder was prepared by a modified Pechini technique with combined EDTA-citric method resulting in nano-sized starting powders. The ceramics were densified by SPS at different sintering temperatures. The focus was on low temperature sintering in order to obtain fine-grained BZY samples. This also avoided the vaporization of the Ba during high temperature sintering. The phase structures and microscrostructures of the proton conductors, as well as the resulting electrical properties of the proton conducting ceramics were investigated.

Experimental

Sample preparation

The proton conducting ceramic powders were prepared by a modified pechini method reported elsewhere [5,28,30]. $Ba(NO_3)_2$ (Alfa Aesar, 99.95%), $Ce(NO_3)_3 \cdot 6H_2O$ (Alfa Aesar, 99.5%), $ZrO(NO_3)_2 \cdot xH_2O$ (Alfa Aesar, 99.9%), $Y(NO_3)_3 \cdot 6H_2O$ (Alfa Aesar, 99.9%) and $Yb(NO_3)_3 \cdot xH_2O$ (Alfa Aesar, 99.9%) starting chemicals were dissolved in deionized water. The concentration of the metal ions in the individual nitrate was determined by titration. Citric acid (Alfa Aesar, 99%) and ethylenediaminetetraacetic acid (EDTA, Alfa Aesar, 99%) were employed as chelating and complexing agents for each composition. Ammonium hydroxide (Sigma–Aldrich, NH_3 content 28.0–30.0%) was added to promote the dissolution of EDTA. The metal precursors were then stoichiometrically added into the chelating and complexing agents with metal nitrates: citric acid: EDTA molar ratio = 1: 1.5: 1.2. At this stage, ammonium hydroxide was added to keep the precursors soluble in the solution. The solution was heated and stirred for 24 h to achieve a fully chelated gel, followed by heat treatment in a kitchen microwave oven to assist in foaming. The gel was burned into foam during the process and the obtained ashes were subsequently fired at 600 °C for 4 h in air to remove the organic residue. The powder was then calcined at 1100 °C to form pure phase BZY powder samples.

The calcined proton conductor powder samples were then sintered by the SPS method. The powders were filled into a graphite die with a diameter of 12.7 mm, and sintered by the SPS machine (Dr. Sinter 1020, Sumitomo Coal Mining Co.). This process was accomplished by applying a constant 4 MPa axial pressures and an increasing AC current (100 A min^{-1}) simultaneously to the die in dynamic vacuum (~10 Pa), while the temperature of sample was monitored by a pyrometer.

Characterization

The crystal structures of the calcined and sintered samples were recorded on an X-ray diffractometer (Rigaku, Japan) with graphite-monochromatized CuKa radiation ($\lambda = 1.5418$ Å) at a scanning rate of 2° min^{-1} in a 2θ range from 20 to 80°. The diffraction patterns were analyzed by performing Rietveld refinement using the General Structure Analysis System (GSAS) package and the graphical user interface (EXP GUI) [24,25]. The surface microstructure and the cross-sectional morphology of the sintered pellets were characterized by scanning electron microscopy (FESEM, Zeiss Ultra). The relative density of the samples was measured by the Archimedes method. For the conductivity measurements, both surfaces of the sintered pellets were polished, painted with platinum paste (Heraeus, CL11-5349) and baked at 950 °C for 30 min. Platinum wires were then attached to the surface of the platinum layer. Electrical conductivity was measured using an A.C. impedance method with an A.C. amplitude of 10 mV in the frequency range from 0.1 Hz to 8 MHz via an electrochemical station with a built-in impedance analyzer (Zahner IM6 Electrochemical Workstation, ZAHNER-Elektrik GmbH & Co., Kronach, Germany). The conductivity measurement was carried out in dry air (dynamic air flowing through a silica gel and a $CaPO_4$ sand), wet air and wet H_2 atmospheres (3% water partial pressure, introduced by passing the gas through a water bubbler at room temperature) in a temperature range of 300–750 °C.

Results and discussion

Microstructures

Fig. 1 displays the cross-sectional microstructures of the BZY samples sintered by SPS at temperatures of 1200, 1300 and 1400 °C, respectively, for 5 min. Samples sintered at 1200 °C exhibit a noticeable level of porosity in proximity to densified regimes. The average grain size was observed to be less than 200 nm. The 1300 °C and 1400 °C sintered samples showed a dense microstructure, with grain sizes of 200 ± 80 nm, and 260 ± 120 nm respectively. A close investigation revealed an oriented distribution of dense and porous layers as shown in Fig. 1(d). The porous layers were forced along the direction perpendicular to the SPS axis. The porous layer will impede the current flow and increase the magnitude of the nominal impedance. The impedance value we obtained here is thus the lower limit of the actual impedance. Higher sintering temperatures (>1400 °C) reduced the overall porosity in the porous layer. This is consistent with our density measurement indicating a relative density of 92.4% for the 1400 °C sintered sample, compared to 85.5% for the 1300 °C sintered sample. The layered distribution of denser and porous layers was attributed to the distribution of the SPS current during sintering [16]. The dense layer with a lower overall resistance may have served as a conduit for current passing through the sample, partially bypassing the more resistive porous layers. For further experiments, only the sample SPS sintered at 1300 and 1400 °C were considered. The sintering conditions of barium zirconate based materials are listed in Table 1 for reference.

XRD analysis

Fig. 2 shows the XRD patterns of the as-synthesized BZY powders calcined at 1100 °C for 10 h, and the SPS samples sintered at 1300 and 1400 °C, respectively. All of the samples display a predominant perovskite structure. In addition to the perovskite peaks, the sample sintered at 1400 °C exhibits an extra graphite peak, attributed to the diffusion of graphite from the die into the sample surface. In the inset of Fig. 2, the peak shift between samples can be clearly identified. The increased sintering temperature resulted in a shift of the XRD peaks to a lower angle, indicating an increase of the lattice parameter with higher sintering temperature. The typical refined XRD pattern of the calcined BZY powder sample is shown in Fig. 3. The samples were fitted with a cubic phase *Pm-3m* space group, without any secondary phases present. A lattice parameters of a = 4.1989 Å was obtained for the powder sample calcined at 1100 °C from the Rietveld refinement. The lattice parameter for 1300 and 1400 °C sintered samples were calculated to be a = 4.20237 and a = 4.21195 Å, respectively. The observed peak shift has been confirmed by adding the peaks of an Al sample holder as the calibration standard. It is known that increasing the effective Y content in the unit cell

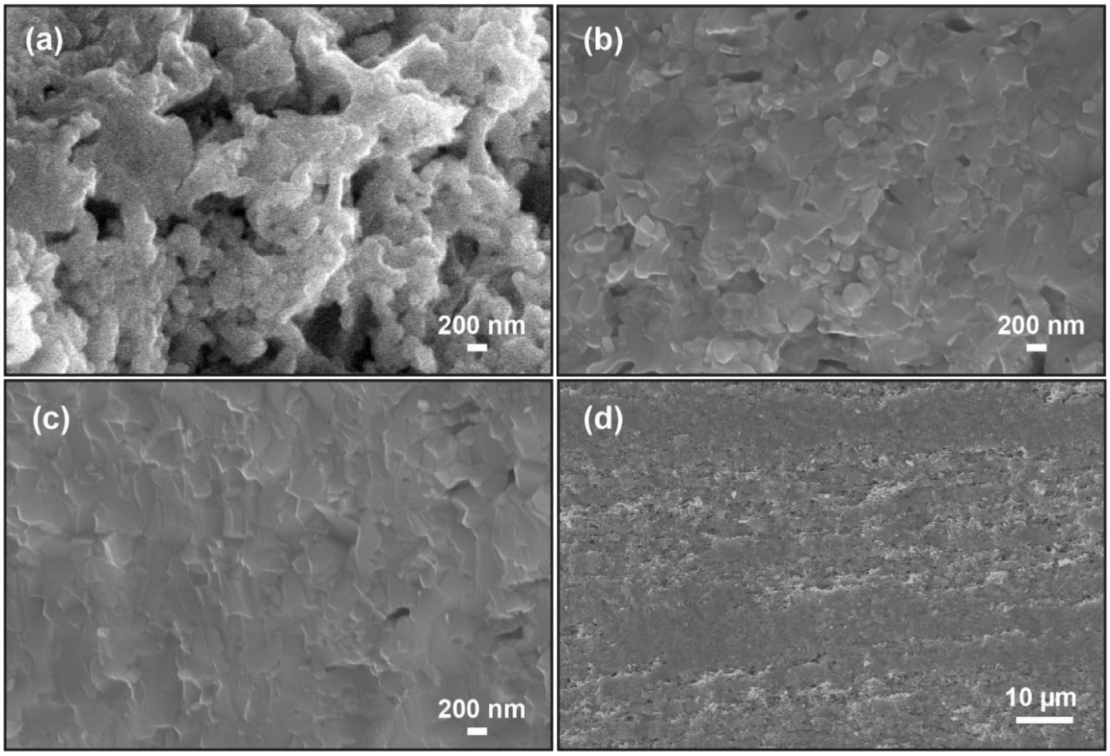

Fig. 1 – SEM cross-section pictures of BZY samples SPS sintered at different temperatures for 5 min, (a) 1200 °C, (b) 1300 °C, and (c) 1400 °C. (d) The low magnified SEM picture of the sample sintered at 130 °C, where layered structure can be observed.

Table 1 – Conductivity values (at 500 °C) and Activation Energy values of BZY samples.

Sample	Sintering condition	Grain size (μm)	Total ($S\ cm^{-1}$)	Grain boundary ($S\ cm^{-1}$)	Bulk ($S\ cm^{-1}$)	Atmos.	Ea (eV)	Ref.
BZY10	1400 °C, 5 min, SPS, nitrates	0.26	9.4×10^{-7}	2.4×10^{-6}	1.6×10^{-6}	Wet H_2	1.20	This work
BZY10	1450 °C, 6 h, acetates	0.2–0.5	7.5×10^{-6}	7.8×10^{-6}	2.6×10^{-4}	Wet 5% H_2/Ar	0.21 (bulk), 0.72 (gb)	Irvine [19]
BZY10	1700 °C, 5 min, SPS, SSR	0.23	1.0×10^{-3}	4.4×10^{-4}	8.4×10^{-4}	Wet 9% H_2/N_2	0.43 (bulk), 0.64 (gb)	Ricote [18]
BZY05	1800 °C, 20 h	0.67	–	8.2×10^{-3}	1.7×10^{-3}	Wet air	–	Iguchi [6]
BZY20-ZnO	1325 °C, 10 h,	–	4.8×10^{-4}	1.5×10^{-3}	7.6×10^{-4}	Wet 5% H_2/Ar	0.23	Irvine [22]
BZY20-Li	1600 °C, 6 h, wet chemistry nitrates	0.43	2.7×10^{-3}	7.4×10^{-4} (350 °C)	3.5×10^{-3} (350 °C)	Wet 10% H_2/Ar	0.48	Traversa [21]
BZY20	1600 °C, 24 h Reactive sintering, nitrates	1	2.2×10^{-2}	1.0×10^{-2} (350 °C)	1.2×10^{-2} (350 °C)	wet N_2 or Ar	–	Haile [31]
BZY20	1500 °C, 20 h, alkoxides	0.2	4×10^{-3}	–	–	Wet Ar	0.54	Cervera [2]

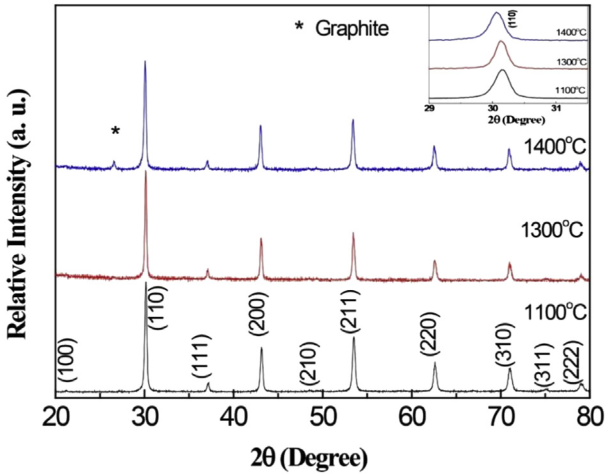

Fig. 2 – XRD patterns of the as synthesized BZY powders calcined at 1100 °C (black line), and polished surface XRD patterns of samples spark plasma sintered 1300 and 1400 °C for 5 min. Inset is the expanded view of (110) peaks for the samples.

increases the lattice parameter due to a combination of the difference in ionic radii and an increased oxygen vacancy content. An additional explanation was proposed by J. Irvine that two variants of BZY, both with cubic perovskite *Pm-3m* structure, with α-phase exhibits smaller unit cell and lower protonic conductivity than the β-phase [1]. It is believed that the cross substitution of Y from B-sites onto the A-sites, including charge compensation which increases oxygen occupancy leads to the increased unit cell size. Surface stress that may exist in the polished sample surfaces that would likely affect the lattice parameter should be not significant and have been ruled out as the origin of the peak shift.

Conductivity

Fig. 4 shows a Nyquist plot of the BZY sample impedance spectrum. The impedance spectrum typically has three semi-

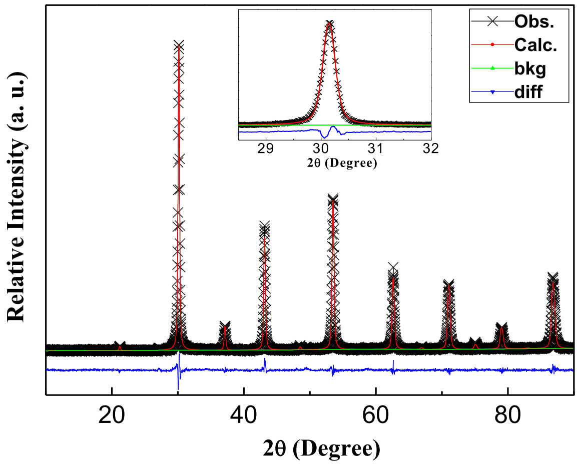

Fig. 3 – Typical Rietveld refined XRD patterns of the as calcined BZY sample, with *Pm-3m* space group, $R_{wp} = 6.32\%$, $R_p = 5.46\%$, $\chi^2 = 1.525$.

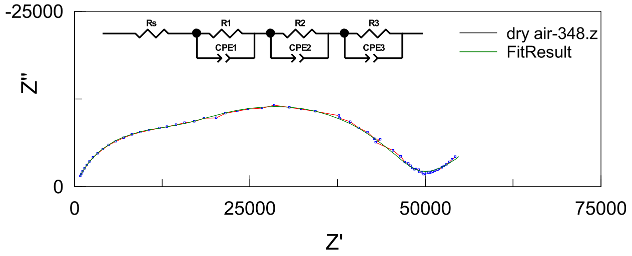

Fig. 4 – Nyquist plots for BZY sample tested in dry air at 348 °C. The fitting was achieved by using a series of R-CPE model.

circles corresponding to the bulk, grain boundary and electrode responses from high to low frequencies, which can be fitted by a parallel R-CPE (constant phase element) equivalent circuit model. The inset in Fig. 4 is the R-CPE model that was used to fit the impedance spectra in the present work.

Fig. 5 shows the Arrhenius plots of the total conductivity as a function of testing temperature for the BZY sample sintered at different temperatures. The tests were conducted in dry air (Fig. 5(a)), wet air (Fig. 5(b)), wet N_2 (Fig. 5(c)), and wet H_2 (Fig. 5(d)), respectively. Overall the conductivity values of the sample sintered at 1300 °C and 1400 °C are similar. However, the sample sintered at 1400 °C displayed slightly higher values of conductivity. This behavior is more predominant at higher temperatures.

The activation energy (E_a) of the samples was obtained by linear fitting the slopes of the Arrhenius plots from equation (1):

$$\sigma T = A*\exp\left(-\frac{E_a}{RT}\right) \tag{1}$$

where σ is the conductivity, T is the temperature in K, A is constant, R is the gas constant. The activation energy is lower for the BZY sample sintered at 1300 °C, especially in the high temperature regime and reducing atmospheres (Fig. 5(d)).

For comparison, the total conductivity of the BZY sample SPS sintered at 1400 °C in different atmospheres is presented in Fig. 6. In the temperature regime below 600 °C, the sample tested in wet H_2 exhibited the highest conductivity and lowest activation energy, while the sample tested in dry air possessed the highest activation energy. The conductivity and activation energy values of this material, which are characteristic of proton conduction, are presented in Table 1.

Fig. 7 shows the Arrhenius plots of the bulk and grain boundary conductivity of samples tested in wet N_2. It was observed that the sample sintered at 1400 °C displayed higher bulk and higher grain boundary conductivity than the sample sintered at 1300 °C.

Fig. 8 shows the bulk and grain boundary (GB) conductivity measured in wet air and wet H_2 for the sample SPS sintered at 1400 °C. The trends observed in the bulk and grain boundary conductivity were similar to those observed for the total

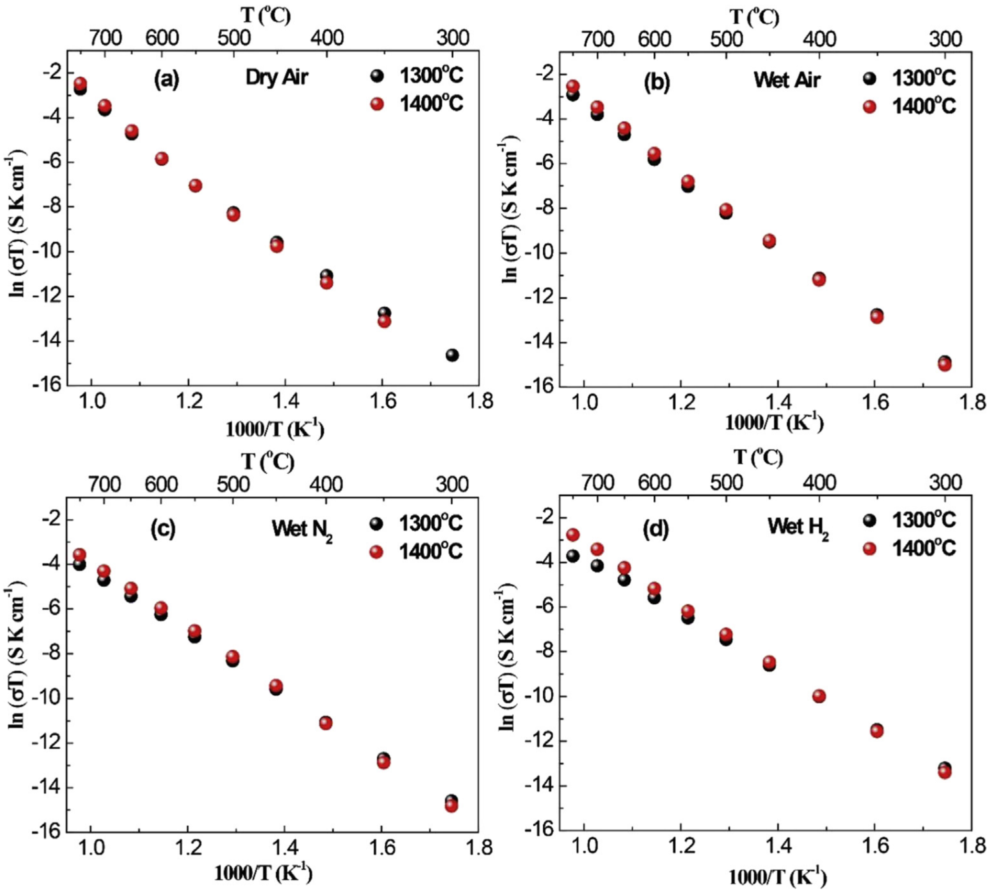

Fig. 5 – Total conductivity of the BZY samples sintered at 1300 and 1400 °C measured in different atmospheres.

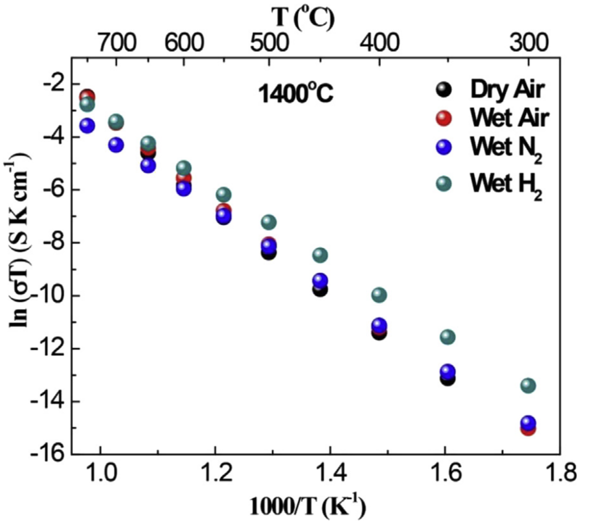

Fig. 6 – Total conductivity of the BZY samples sintered at 1400 °C in different atmospheres.

conductivity. The bulk and grain boundary conductivity values were smaller in wet H_2, with lower activation energy due to the significant p-type electronic conduction present in oxidizing atmospheres [17]. The activation energy of the grain boundary conduction was observed to be higher than the bulk conduction, which results in the grain boundary conductivity becoming dominant at higher temperatures. This observation is consistent with the literature results shown in Table 1.

It is noted that the conductivity and activation energy of the samples prepared in this work were lower than the Barium Zirconate based materials prepared elsewhere. The conductivity values of our samples sintered via the SPS method is ~2–3 orders of magnitude lower compared to literature results on varying $BaZr_{1-x}Y_xO_{3-\delta}$ compositions. For example, $BaZr_{0.8}Y_2O_{3-\delta}$ (BZY20) samples prepared by a solid state reaction method sintered in the range of 1325–1600 °C in the presence of sintering aids displayed ~2–3 order of magnitude higher conductivity than the present work [21,23]. In addition, BZY materials sintered via a solid state reaction method at 1600 °C for 24 h resulted in conductivity values ~4 order of magnitude greater than the present work [31]. It is apparent that the effective Y dopant concentration in the structure should be taken into consideration when interpreting the results. The samples prepared in this study contained only 10% Y dopant, and the conductivity values were similar with BZY samples sintered at 1450 °C by a sol–gel method, which has a typical grain size of 200–500 nm [19].

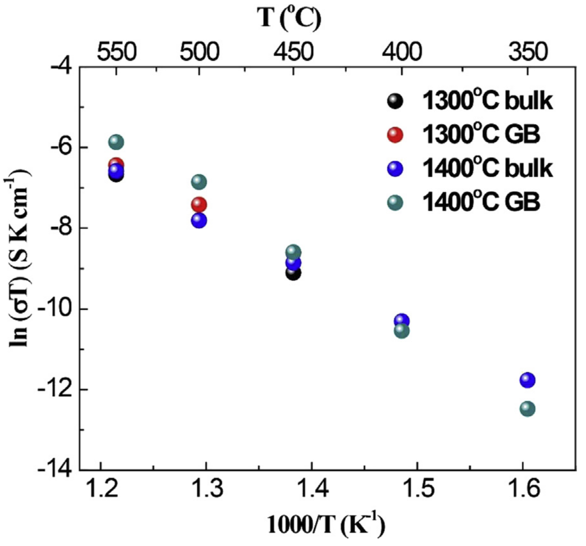

Fig. 7 – Comparison of the bulk and grain boundary (GB) conductivity in wet N_2 for the BZY samples sintering at 1300 and 1400 °C.

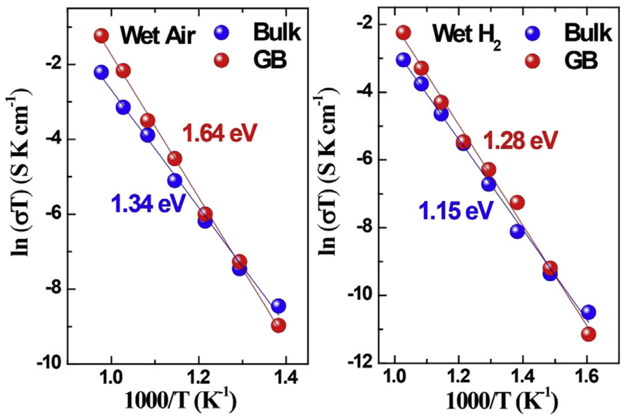

Fig. 8 – Bulk and grain boundary (GB) conductivity for BZY sample sintered at 1400 °C.

The observed reduction in grain boundary conductivity can be understood by considering the SPS induced microstructure, which consists of a large number of grain boundaries due to the lowed sintering temperature and short sintering time of the SPS method. As can be seen from the SEM pictures, the grain sizes of our samples was approximately 200–400 nm, compared to ~1 μm for the samples prepared via the other methods mentioned above. At the same time, the grain boundary and bulk activation energy value of the sample in our experiment was also higher than the literature results indicating an additional electronic conduction component along with the ionic conduction in our materials.

The exact reason for the lowered bulk conductivity is not clear at present. It was observed by Irvine et al., that higher sintering temperatures produce more of a β-phase in polymorphic BZY. The Y doping on the A-site reduces the overall oxygen vacancy content and replaces negative charged defects on the B-site, Y'_{Zr}, with positively charged defects on the A site $Y^{\bullet}_{Ba}$, decreasing defect association [1,3,17]. We attempted to look at this phenomenon in our work, but due to the low resolution of the XRD used in our experiments, it was difficult to observe differences due to these effects in our samples. Future work will involve the use of more sensitive neutron powder diffraction experiments to study this phenomenon. However, we currently believe the β-phase may contribute to the change in the bulk conductivity for our samples. For example, increasing the SPS treatment temperature up to 1700 °C for 5 min for BZY samples prepared by a solid state reaction method resulted in conductivity values of ~10^{-3} S cm^{-1} at 600 °C [18]. These values of conductivity are ~3 orders of magnitude higher than our results and comparable to the best results reported on this material system. At present, it is believed that the high sintering temperature is more favorable for the formation of a β-phase which is expected to possess higher proton conductivity.

Conclusions

$BaZr_{0.9}Y_{0.1}O_3$ ceramic powders were successfully prepared by a modified pechini method at 1100 °C. SPS of the samples at 1300–1400 °C for 5 min was sufficient to obtain densified, fine grained microstructure due to the enhanced kinetics for SPS densification. The sintered samples were pure phase, and exhibited an increase in the lattice parameter with increasing sintering temperature. The sample sintered at 1400 °C exhibited higher conductivity than samples sintered at 1300 °C. The 1400 °C sintered sample displayed a lower grain boundary conductivity of 2.4×10^{-6} S cm^{-1} at 500 °C, and a higher activation energy of 1.28 eV, compared with literature results from conventionally prepared materials, which was due to the ultra-fined microstructure of the sample prepared by SPS. This large grain boundary area was used as a "tool" to investigate the interfacial conduction in these materials systems. The bulk conductivity was also lower than the reported data, with values approaching 1.6×10^{-6} S cm^{-1} at 500 °C, which was ascribed to variations in the relative amounts of the β-phase in BZY polymorphs sintered at lower temperatures.

Acknowledgment

The authors acknowledge financial support from an Energy Frontier Research Center on Science Based Nano-Structure Design and Synthesis of Heterogeneous Functional Materials for Energy Systems (HeteroFoaM Center) funded by the U.S. Department of Energy, Office of Science, Office of Basic Energy Sciences (Award no. DE-SC0001061). K. Brinkman and J. He also wishes to acknowledge a 2014 Clemson TIGER Grant on Materials and Processes for Natural Gas Utilization.

REFERENCES

[1] Azad AK, Savaniu C, Tao S, Duval S, Holtappels P, Ibberson RM, et al. Structural origins of the differing grain conductivity values in $BaZr_{0.9}Y_{0.1}O_{2.95}$ and indication of novel approach to counter defect association. J Mater Chem 2008;18(29):3414–8.

[2] Cervera RB, Oyama Y, Miyoshi S, Kobayashi K, Yagi T, Yamaguchi S. Structural study and proton transport of bulk nanograined Y-doped $BaZrO_3$ oxide protonics materials. Solid State Ionics 2008;179(7–8):236–42.

[3] Duval SBC, Holtappels P, Vogt UF, Stimming U, Graule T. Characterisation of $BaZr_{0.9}Y_{0.1}O_{3-\delta}$ prepared by three different synthesis methods: study of the sinterability and the conductivity. Fuel Cells 2009;9(5):613–21.

[4] Fabbri E, Bi L, Tanaka H, Pergolesi D, Traversa E. Chemically stable Pr and Y Co-doped barium zirconate electrolytes with high proton conductivity for intermediate-temperature solid oxide fuel cells. Adv Funct Mater 2011;21(1):158–66.

[5] Fang S, Wang S, Brinkman KS, Chen F. A sinteractive Ni-$BaZr_{0.8}Y_{0.2}O_{3-\delta}$ composite membrane for hydrogen separation. J Mater Chem A 2014;2(16):5825–33.

[6] Iguchi F, Yamada T, Sata N, Tsurui T, Yugami H. The influence of grain structures on the electrical conductivity of a $BaZr_{0.95}Y_{0.05}O_3$ proton conductor. Solid State Ionics 2006;177(26–32):2381–4.

[7] Iwahara H, Esaka T, Uchida H, Maeda N. Proton conduction in sintered oxides and its application to steam electrolysis for hydrogen production. Solid State Ionics 1981;3–4:359–63.

[8] Jing Y, Ma Y, Patakangas J, Zhu B, Johnsson M, Cura ME, et al, "Enhanced conductivity of SDC based nanocomposite electrolyte by spark plasma sintering," *Int J Hydrogen Energy*, 39(26):14391–14396.

[9] Kjølseth C, Fjeld H, Prytz Ø, Dahl PI, Estournès C, Haugsrud R, et al. Space–charge theory applied to the grain boundary impedance of proton conducting $BaZr_{0.9}Y_{0.1}O_{3-\delta}$. Solid State Ionics 2010;181(5–7):268–75.

[10] Kreuer KD. Proton-conducting oxides. Annu Rev Mater Res 2003;33:333–59.

[11] Lan R, Tao S. Novel proton conductors in the layered oxide material $Li_xlAl_{0.5}Co_{0.5}O_2$. Adv Energy Mater 2014;4(7):1301683.

[12] Liu B, Zhang Y. $La_{0.9}Sr_{0.1}Ga_{0.8}Mg_{0.2}O_{3-\delta}$ sintered by spark plasma sintering (SPS) for intermediate temperature SOFC electrolyte. J Alloys Compd 2008;458(1–2):383–9.

[13] Maglia F, Anselmi-Tamburini U, Chiodelli G, Çamurlu HE, Dapiaggi M, Munir ZA. Electrical, structural, and microstructural characterization of nanometric $La_{0.9}Sr_{0.1}Ga_{0.8}Mg_{0.2}O_{3-\delta}$ (LSGM) prepared by high-pressure spark plasma sintering. Solid State Ionics 2009;180(1):36–40.

[14] Pergolesi D, Fabbri E, D'Epifanio A, Di Bartolomeo E, Tebano A, Sanna S, et al. High proton conduction in grain-boundary-free yttrium-doped barium zirconate films grown by pulsed laser deposition. Nat Mater 2010;9(10):846–52.

[15] Rajeswari K, Suresh MB, Chakravarty D, Das D, Johnson R. Effect of nano-grain size on the ionic conductivity of spark plasma sintered 8YSZ electrolyte. Int J Hydrogen Energy 2012;37(1):511–7.

[16] Ramirez C, Figueiredo FM, Miranzo P, Poza P, Osendi MI. Graphene nanoplatelet/silicon nitride composites with high electrical conductivity. Carbon 2012;50(10):3607–15.

[17] Ricote S, Bonanos N, Manerbino A, Coors WG. Conductivity study of dense $BaCe_xZr_{(0.9-x)}Y_{0.1}O_{(3-\delta)}$ prepared by solid state reactive sintering at 1500 °C. Int J Hydrogen Energy 2012;37(9):7954–61.

[18] Ricote S, Bonanos N, Wang HJ, Boukamp BA. Conductivity study of dense $BaZr_{0.9}Y_{0.1}O_{(3-\delta)}$ obtained by spark plasma sintering. Solid State Ionics 2012;213(0):36–41.

[19] Savaniu CD, Canales-Vazquez J, Irvine JTS. Investigation of proton conducting $BaZr_{0.9}Y_{0.1}O_{2.95}$: $BaCe_{0.9}Y_{0.1}O_{2.95}$ core-shell structures. J Mater Chem 2005;15(5):598–604.

[20] Sun W, Liu M, Liu W. Chemically stable yttrium and tin Co-doped barium zirconate electrolyte for next generation high performance proton-conducting solid oxide fuel cells. Adv Energy Mater 2013;3(8):1041–50.

[21] Sun Z, Fabbri E, Bi L, Traversa E. Lowering grain boundary resistance of $BaZr_{0.8}Y_{0.2}O_{3-\delta}$ with $LiNO_3$ sintering-aid improves proton conductivity for fuel cell operation. Phys Chem Chem Phys 2011;13(17):7692–700.

[22] Tao S, Irvine JTS. Conductivity studies of dense yttrium-doped $BaZrO_3$ sintered at 1325 °C. J Solid State Chem 2007;180(12):3493–503.

[23] Tao SW, Irvine JTS. A stable, easily sintered proton-conducting oxide electrolyte for moderate-temperature fuel cells and electrolyzers. Adv Mater 2006;18(12):1581–4.

[24] Toby B. EXPGUI, a graphical user interface for GSAS. J Appl Crystallogr 2001;34(2):210–3.

[25] Wang S, Chen Y, Fang S, Zhang L, Tang M, An K, et al. Novel chemically stable $Ba_3Ca_{1.18}Nb_{1.82-x}Y_xO_{9-\delta}$ proton conductor: improved proton conductivity through tailored cation ordering. Chem Mater 2014;26(6):2021–9.

[26] Wang S, Zhang L, Yang Z, Zhang L, Fang S, Brinkman K, et al. Two-step co-sintering method to fabricate anode-supported $Ba_3Ca_{1.18}Nb_{1.82}O_{9-\delta}$ proton-conducting solid oxide fuel cells. J Power Sources 2012;215:221–6.

[27] Wang S, Zhang L, Zhang L, Brinkman K, Chen F. Two-step sintering of ultrafine-grained barium cerate proton conducting ceramics. Electrochim Acta 2013;87(0):194–200.

[28] Wang S, Zhao F, Zhang L, Brinkman K, Chen F. Stability and electrical property of $Ba_{1-x}Sr_xCe_{0.8}Y_{0.2}O_{3-\delta}$ high temperature proton conductor. J Alloys Compd 2010;506(1):263–7.

[29] Wang S, Zhao F, Zhang L, Brinkman K, Chen F. Doping effects on complex perovskite $Ba_3Ca_{1.18}Nb_{1.82}O_{9-\delta}$ intermediate temperature proton conductor. J Power Sources 2011;196(19):7917–23.

[30] Wang S, Zhao F, Zhang L, Chen F. Synthesis of $BaCe_{0.7}Zr_{0.1}Y_{0.1}Yb_{0.1}O_{3-\delta}$ proton conducting ceramic by a modified Pechini method. Solid State Ionics 2012;213(0):29–35.

[31] Yamazaki Y, Hernandez-Sanchez R, Haile SM. High total proton conductivity in large-grained yttrium-doped barium zirconate. Chem Mater 2009;21(13):2755–62.

[32] Yang L, Wang SZ, Blinn K, Liu MF, Liu Z, Cheng Z, et al. Enhanced sulfur and coking tolerance of a mixed ion conductor for SOFCs: $BaZr_{0.1}Ce_{0.7}Y_{0.2-x}Yb_xO_{3-\delta}$. Science 2009;326(5949):126–9.

[33] Zhang L, Mao Z, Thomason JD, Wang S, Huang K. Synthesis of a homogeneously porous solid oxide matrix with tunable porosity and pore size. J Am Ceram Soc 2012;95(6):1832–7.

[34] Zhao F, Wang S, Dixon L, Chen F. Novel $BaCe_{0.7}In_{0.2}Yb_{0.1}O_{3-\delta}$ proton conductor as electrolyte for intermediate temperature solid oxide fuel cells. J Power Sources 2011;196(18):7500–4.